

Optimum parameters and performance of tuned mass damper-inerter for base-isolated structures

Radhey Shyam Jangid*

Department of Civil Engineering, Indian Institute of Technology Bombay, Powai, Mumbai - 400 076, India

(Received March 28, 2021, Revised August 30, 2021, Accepted December 27, 2021)

Abstract. The optimum damping and tuning frequency ratio of the tuned mass damper-inerter (TMDI) for the base-isolated structure is obtained using the numerical searching technique under stationary white-noise and filtered white-noise earthquake excitation. The minimization of the isolated structure's mean-square relative displacement and absolute acceleration, as well as the maximization of the energy dissipation index, were chosen as the criteria for optimality. Using a curve-fitting technique, explicit formulae for TMDI damping and tuning frequency for white-noise excitation are then derived. The proposed empirical expressions for TMDI parameters are found to have a negligible error, making them useful for the effective design of base-isolated structures. The effectiveness of TMDI and its optimum parameters are influenced by the soil condition and isolation frequency, according to the comparison made of the optimized parameters and response with different soil profiles. The effectiveness of an optimally designed TMDI in controlling the displacement and acceleration response of the flexible isolated structure under real and pulse-type earthquakes is also observed and found to be increased as the inertance mass ratio increases.

Keywords: cycloidal pulses; filtered white-noise; floor accelerations; optimum parameters; seismic base isolation; stationary excitation; tuned mass damper-inerter

1. Introduction

During earthquakes, seismic base isolation is an effective way to protect structures and their contents. To reduce the damage of civil engineering structures due to earthquakes, several types of base isolation systems have been developed over the last 40 years. Full-scale applications of some of the base-isolated systems have been done in new design and retrofit of strategic buildings, such as hospitals, barracks, firehouses, emergency management headquarters, etc. (Spencer and Nagarajaiah 2003, Matsagar and Jangid 2008, Tiong *et al.* 2017). One of the major concerns in base-isolated structures is to reduce the isolator displacement for ensuring their safety and stability during strong seismic events. To control the isolator displacement, supplemental devices such as viscous, visco-elastic, friction, magnetorheological, piezoelectric friction, negative stiffness, variable dampers, shape memory alloy dampers, etc. along with base isolation system had been proposed and studied (Makris and Chang 2000a, Lin *et al.* 2006, Reigles and Symans 2006, Kataria and Jangid 2016, Madhekar and Jangid 2009, Nagarajaiah and Sen 2020, Li and Li 2019, Wang *et al.* 2020). The ability of these dampers to control the seismic response of isolated structures was demonstrated. Recently, Mazza (2019) investigated the effects of the long-term behavior of isolation devices on the seismic response of base-isolated buildings. Furthermore,

the seismic performance of hospital buildings retrofitted with base isolation is also evaluated by comparing to the in-plane-out-of-plane seismic collapse of masonry infills to see if this type of intervention can also preserve the hospital's ability to function after rare earthquakes (Mazza 2021).

Recently, inerter-based damping systems have become popular for vibration control of civil engineering structures. It is two end elements with a large mass amplifying effect due to its inertia whose resisting force is proportional to the relative acceleration between two ends. Due to very large amplification in the apparent inertial mass, it has been combined with a tuned mass damper (TMD) (Garrido *et al.* 2013, Marian and Giaralis 2014, Hu *et al.* 2015, Pietrosanti *et al.* 2017, Masri and Caffrey 2017, Barredo *et al.* 2019, Cao and Li 2019, Cao *et al.* 2020). It was shown that the inerter can store a significant amount of energy from the externally applied forces with very little self-weight and that the performance of the TMD with inerter was significantly improved. The performance of inertial devices as a damper was also studied in building structures (Hwang *et al.* 2007, Lazar 2014, Wen *et al.* 2017, Makris and Moghimi 2019). The improvement in the performance of buildings was also observed with inerter device. Recently, the performance of base-isolated structures assisted with tuned mass damper-inerter (TMDI) attached to the isolation floor was investigated (De Domenico and Ricciardi 2018a, b, Di Matteo *et al.* 2019, De Angelis *et al.* 2019). The TMDI has been shown to mitigate the response of linear and bi-linear isolators to both recorded and stochastic earthquake excitation. The control effectiveness of the TMDI, when installed on the upper floors of the isolated structure was also recently investigated (Li *et al.* 2021). De

*Corresponding author, Ph.D., Professor,
E-mail: rsjangid@civil.iitb.ac.in

Domenico *et al.* (2020) studied the seismic performance of tuned fluid inerter for the structures with friction pendulum isolators. Despite the above studies of TMDI for base-isolated structures, there is further need to study the optimum parameters of the TMDI under various optimization criteria subjected to white-noise and filtered white-noise earthquake excitation and the performance of the optimally designed TMDI under real and cycloidal pulse excitation.

In the present study, the optimum parameters and control effectiveness of the TMDI for the base-isolated structure are studied. The specific objectives of the present study are to (i) present the response analysis of base-isolated structure with supplemental TMDI under stationary earthquake excitation, (ii) obtain the optimum parameters using the numerical searching technique, (iii) derive the explicit equations for the optimum parameters of the TMDI using curve-fitting techniques, (iv) study the effectiveness of TMDI in controlling the seismic response under various soil types, and (v) to study the controlling effects of TMDI devices for base-isolated building under real earthquakes and cycloidal pulses.

2. Rigid base-isolated structure with TMDI

Fig. 1 presents a rigid mass model of a multi-story building with base isolation supplemented with TMDI. The mass, m represents the superstructure mass and that of the base floor above the isolation system. The behavior of the isolation system in the present study considers equivalent linear force-deformation with viscous damping. The equivalent stiffness and damping are denoted by k_b and c_b , respectively. TMDI device consists of an auxiliary mass (m_t), stiffness (k_t), and damper (c_t) referred to as TMD, and an inertial device with inertance as b . The two terminals of the inertial device are connected to the auxiliary mass and the ground. To a reasonable approximation, the movement of the inertial device produces a reaction force proportional to the relative acceleration between the two terminals. The inertance, also known as apparent mass, is a proportional coefficient that could be multiple times the inerter's self-weight. The resonance in the TMD is caused by the vibration of the base-isolated structures, which absorbs the energy through damping devices attached to the damper mass. The base isolation system is defined by the two parameters, namely, isolation period T_b and damping ratio ξ_b defined as

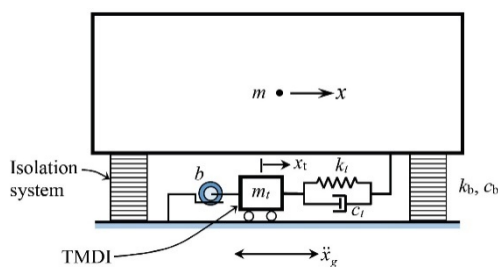


Fig. 1 Structural model of a rigid base-isolated building supplemented with TMDI

$$T_b = \frac{2\pi}{\omega_b}, \quad \omega_b = \sqrt{\frac{k_b}{m}} \quad \text{and} \quad 2\xi_b\omega_b = \frac{c_b}{m} \quad (1)$$

The auxiliary and inertial masses of the TMDI are defined as

$$\mu_t = \frac{m_t}{m}, \quad \mu_b = \frac{b}{m} \quad \text{and} \quad \mu = \mu_t + \mu_b = \frac{m_t + b}{m} \quad (2)$$

The stiffness and damping of the TMDI system are expressed as

$$\xi_t = \frac{c_t}{2(m_t + b)\omega_t}, \quad \omega_t = \sqrt{\frac{k_t}{m_t + b}} \quad \text{and} \quad f = \frac{\omega_t}{\omega_b} \quad (3)$$

where ξ_t denotes the damping ratio of the TMDI; and f denotes the tuning frequency ratio.

The TMDI system for a base-isolated structure can be fully characterized by the parameters μ_t , μ , ξ_t , and f . The TMDI is most effective for lower values of μ_t and higher values of μ and is therefore considered $\mu_t = 0.01$ for all parametric variations in the present study (Pietrosanti *et al.* 2017).

The governing equations of motion can be expressed as

$$\begin{bmatrix} m & 0 \\ 0 & m_t + b \end{bmatrix} \begin{Bmatrix} \ddot{x} \\ \ddot{x}_t \end{Bmatrix} + \begin{bmatrix} c_b + c_t & -c_t \\ -c_t & c_t \end{bmatrix} \begin{Bmatrix} \dot{x} \\ \dot{x}_t \end{Bmatrix} + \begin{bmatrix} k_b + k_t & -k_t \\ -k_t & k_t \end{bmatrix} \begin{Bmatrix} x \\ x_t \end{Bmatrix} = - \begin{Bmatrix} m \\ m_t \end{Bmatrix} (\ddot{x}_g) \quad (4)$$

where x and x_t denotes the displacement relative to the ground of the isolated structure and auxiliary mass of TMDI, respectively; and \ddot{x}_g denotes the input earthquake acceleration. A dot over symbols signifies differentiation to time t .

2.1 Response under White-noise Excitation

By rewriting Eq. (4) as a system of first-order differential equations

$$\dot{\mathbf{Y}} = \mathbf{H}\mathbf{Y} + \mathbf{W} \quad (5)$$

where \mathbf{Y} denotes the state vector; \mathbf{H} denotes the augmented system matrix; and \mathbf{W} represents the excitation vector.

The vectors \mathbf{Y} and \mathbf{W} can be written as

$$\mathbf{Y} = \{x \quad \dot{x} \quad x_t \quad \dot{x}_t\}^T \quad (6)$$

$$\mathbf{W} = \left\{ 0 \quad 0 \quad 1 \quad \frac{m_t}{m_t + b} \right\}^T \ddot{x}_g = \mathbf{B}\ddot{x}_g \quad (7)$$

The augmented response vector \mathbf{Y} is a Markov process, and the corresponding covariance matrix \mathbf{V} satisfies the following equation (Roberts and Spanos 1990)

$$\dot{\mathbf{V}} = \mathbf{H}\mathbf{V}^T + \mathbf{V}\mathbf{H}^T + \mathbf{P} \quad (8)$$

where \mathbf{V}^T is the transpose of matrix \mathbf{V} .

The elements of matrices \mathbf{V} and \mathbf{P} can be written as

$$\mathbf{V}_{ij} = E[\mathbf{Y}_i\mathbf{Y}_j] \quad \text{and} \quad \mathbf{P}_{ij} = E[\mathbf{W}_i\mathbf{W}_j] \quad (9)$$

where E denotes the expectation operator; and \mathbf{Y}_i and \mathbf{W}_i denote the i^{th} element of the vector \mathbf{Y} and \mathbf{W} , respectively.

The input earthquake acceleration \ddot{x}_g is assumed as a Gaussian zero-mean white-noise random process with constant power spectral density function (PSDF) as S_0 . Therefore, the matrix \mathbf{P} can be written as

$$\mathbf{P} = 2\pi S_0 \mathbf{B}\mathbf{B}^T \quad (10)$$

Under the assumption of stationarity, the $\dot{\mathbf{V}}$ will become a null matrix and the solution of the Eq. (8) will provide the \mathbf{V} matrix which will also be the stationary response of the base-isolated structure with TMDI. The elements of the \mathbf{V} matrix represent the values of the required mean-square response such as mean-square relative displacement (σ_x^2) and absolute acceleration ($\ddot{x}_a = \ddot{x} + \ddot{x}_g$) as ($\sigma_{\ddot{x}_a}^2$) of the isolated structure. These mean-square responses are further normalized by dividing the corresponding response of base-isolated structure without TMDI i.e.

$$\tilde{\sigma}_x^2 = \frac{\sigma_x^2}{\sigma_{x,0}^2} \quad \text{and} \quad \tilde{\sigma}_{\ddot{x}_a}^2 = \frac{\sigma_{\ddot{x}_a}^2}{\sigma_{\ddot{x}_a,0}^2} \quad (11)$$

$$\sigma_{x,0}^2 = \frac{\pi S_0}{2\xi_b \omega_b^3} \quad \text{and} \quad \sigma_{\ddot{x}_a,0}^2 = \pi S_0 \omega_b \left(\frac{1}{2\xi_b} + 2\xi_b \right) \quad (12)$$

As a result, values less than unity indicate that the TMDI is effective in reducing response. Further, the performance of the TMDI is also studied based on the energy criterion (Pietrosanti *et al.* 2017). The TMDI is at its best when it can dissipate as much of the total energy input induced by an earthquake excitation as possible. The energy dissipation index is defined as

$$EDI = \frac{E[\Delta E_T]}{E[\Delta E_b] + E[\Delta E_T]} \quad (13)$$

where $E[\Delta E_T]$ and $E[\Delta E_b]$, respectively, denote the expected value of the incremental dissipated energy in the TMDI's viscous element and the base-isolated structure's viscous damping.

The EDI is a variable that ranges from zero to one; it increases as the TMDI's dissipative capacities increase. The EDI is related to the elements of the \mathbf{V} matrix and written as

$$EDI = \frac{c_t \sigma_{\dot{x}_r}^2}{c_b \sigma_x^2 + c_t \sigma_{\dot{x}_r}^2} \quad (14)$$

where σ_x^2 and $\sigma_{\dot{x}_r}^2$ denotes the variances of the velocity \dot{x} and $\dot{x}_r = \dot{x}_t - \dot{x}$, respectively.

3. Optimum TMDI parameters under white-noise excitation

For the given value of μ the optimum TMDI parameters like ξ_t and f are determined. The optimization problem can be written as

$$\text{minimize } \tilde{\sigma}_x^2 \quad \text{subject to } \xi_t \in \Omega_\xi, f \in \Omega_f \quad (15a)$$

$$\text{minimize } \tilde{\sigma}_{\ddot{x}_a}^2 \quad \text{subject to } \xi_t \in \Omega_\xi, f \in \Omega_f \quad (15b)$$

$$\text{maximize } EDI \quad \text{subject to } \xi_t \in \Omega_\xi, f \in \Omega_f \quad (15c)$$

where Ω_ξ and Ω_f represent the feasible regions for ξ_t and f denotes the positive orthants for the associated variables, respectively. To achieve the desired accuracy, an automated numerical search algorithm is used, with ξ_t and f spanning their ranges with increments of 10^{-4} .

For the minimization of $\tilde{\sigma}_x^2$, the optimum parameters and corresponding results of the TMDI are presented in Table 1. It can be noted from this table that the ξ_t^{opt} increase whereas f^{opt} decrease by increasing the μ . The corresponding $\tilde{\sigma}_x^2$ and $\tilde{\sigma}_{\ddot{x}_a}^2$ decrease with the increase of μ implying more effectiveness for higher value of inertance. However, the corresponding reduction due to TMDI for $\mu > 0.4$ is marginal only. The EDI increases as the value of μ increases. Table 1 also presents the corresponding results for the minimization of $\tilde{\sigma}_{\ddot{x}_a}^2$. The main difference is that the optimal values of ξ_t and f obtained by minimizing acceleration are usually higher than those obtained by minimizing displacement. Further, Table 1 reveals that the optimum parameters for the maximization of the EDI are observed to be bounded between the optimum parameters for the minimization of $\tilde{\sigma}_x^2$ and $\tilde{\sigma}_{\ddot{x}_a}^2$ for the practical range of the inertance-mass ratio.

3.1 Closed-form equations of optimum TMDI parameters

For ease of use in engineering applications, explicit mathematical expressions that correspond to the optimum parameters of the TMDI system are obtained using the numerical searching technique. Determining exact closed-form expressions for the optimum TMDI parameters is extremely difficult, and it becomes even more difficult after applying the optimization conditions for the base-isolated structure. As a result, a curve-fitting scheme is applied to the numerical values of the optimum TMDI parameters to obtain explicit expressions for the optimum TMDI parameters. The optimum parameters reported in Table 1 are the functions of μ only for a specified isolation damping ratio (i.e., $\xi_b = 0.1$). Some of the past studies have reported the expression for the classical damped main system (Bakre and Jangid 2007, Patil and Jangid 2011, Tigli 2012, Bandivadekar and Jangid 2013, Salvi and Rizzi 2016) and similar equations were tried currently. The equations of the optimum damping and tuning of the TMDI were examined for the minimum mean square error. The following expressions for the optimum parameters of the TMDI for three different optimization conditions are obtained after several trials and errors.

For minimization of $\tilde{\sigma}_x^2$

$$\xi_t^{opt} = \sqrt{\frac{\mu(4 + 3\mu)}{8(1 + \mu)(2 + \mu)}} \quad (16)$$

$$f^{opt} = 0.97 \left(\frac{\sqrt{1 + \mu/2}}{1 + \mu} \right) \quad (17)$$

Table 1 TMDI parameters that are optimal for various values of parameter μ and optimization criteria ($\xi_b = 0.1$)

μ	Minimization of $\tilde{\sigma}_x^2$			Minimization of $\tilde{\sigma}_{x_a}^2$			Maximization of EDI		
	ξ_t^{opt}	f^{opt}	$\tilde{\sigma}_x^2$	ξ_t^{opt}	f^{opt}	$\tilde{\sigma}_{x_a}^2$	ξ_t^{opt}	f^{opt}	EDI
0.02	0.0697	0.95004	0.840	0.0741	1.00652	0.831	0.0713	0.97816	0.175
0.03	0.0856	0.94713	0.796	0.0939	1.01477	0.786	0.0881	0.98066	0.220
0.04	0.0984	0.9427	0.760	0.1109	1.01946	0.751	0.1026	0.98047	0.256
0.05	0.1097	0.93661	0.731	0.1267	1.022	0.721	0.1152	0.97876	0.287
0.06	0.1197	0.93039	0.706	0.1412	1.02406	0.695	0.1268	0.97667	0.314
0.085	0.1414	0.91504	0.656	0.1748	1.02595	0.642	0.152	0.96981	0.368
0.11	0.1597	0.89957	0.617	0.2051	1.02519	0.601	0.1739	0.96165	0.410
0.16	0.1898	0.87065	0.559	0.261	1.01896	0.538	0.2125	0.9447	0.474
0.21	0.2134	0.84356	0.517	0.3116	1.00984	0.493	0.2449	0.92795	0.521
0.26	0.2336	0.81886	0.484	0.3584	0.99754	0.458	0.2744	0.91142	0.559
0.31	0.2514	0.7958	0.457	0.401	0.98326	0.430	0.3009	0.89592	0.590
0.36	0.2673	0.77439	0.435	0.4392	0.96678	0.408	0.3261	0.88048	0.616
0.41	0.281	0.75464	0.415	0.473	0.94756	0.390	0.3494	0.86631	0.638
0.46	0.2938	0.73621	0.399	0.5013	0.92834	0.376	0.3717	0.85213	0.658
0.51	0.3052	0.71869	0.384	0.5277	0.90565	0.365	0.3924	0.83891	0.675
0.61	0.3259	0.68759	0.359	0.5678	0.8613	0.349	0.4312	0.81371	0.705
0.71	0.3434	0.65943	0.339	0.5979	0.81208	0.340	0.4674	0.791	0.729
0.81	0.3582	0.63441	0.321	0.6216	0.76065	0.335	0.5012	0.76999	0.749
0.91	0.3712	0.61226	0.307	0.6437	0.70625	0.333	0.5331	0.75023	0.766
1.01	0.3835	0.59153	0.294	0.6705	0.64921	0.333	0.5634	0.73211	0.781

For minimization of $\tilde{\sigma}_{x_a}^2$

$$\xi_t^{opt} = \sqrt{\mu}(0.3584 + 1.0765\sqrt{\mu} - 0.7628\mu) \quad (18)$$

$$f^{opt} = \sqrt{1 - \frac{\mu}{2}}(0.9716 + 0.4492\sqrt{\mu} - 0.4828\mu) \quad (19)$$

For maximization of EDI

$$\xi_t^{opt} = \frac{\sqrt{\mu}}{2}(1 + 0.1226\sqrt{\mu}) \quad (20)$$

$$f^{opt} = \frac{1}{\sqrt{1 + \mu}}(1 + 0.0483\sqrt{\mu}) \quad (21)$$

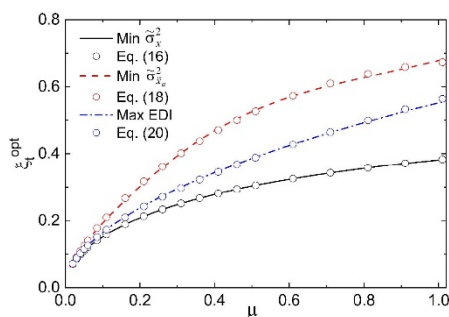


Fig. 2 Comparison of the optimum TMDI damping of base-isolated structure with proposed empirical equations

Figs. 2 and 3 present the comparison of the optimum parameters of the TMDI obtained using the numerical searching technique and the proposed empirical equations as above. The optimum parameters of the TMDI by the two approaches are found to be in good agreement in these figures. Thus, the explicit equations proposed for the optimum TMDI parameters for base-isolated structures using the curve-fitting scheme fit well.

A comparison of the $\tilde{\sigma}_x^2$, $\tilde{\sigma}_{x_a}^2$ and EDI obtained using the numerical search technique and by using the proposed empirical equations of the optimum TMDI parameters is shown in Fig. 4. The figure reveals that the $\tilde{\sigma}_x^2$, $\tilde{\sigma}_{x_a}^2$ and EDI are matching well when obtained by the TMDI

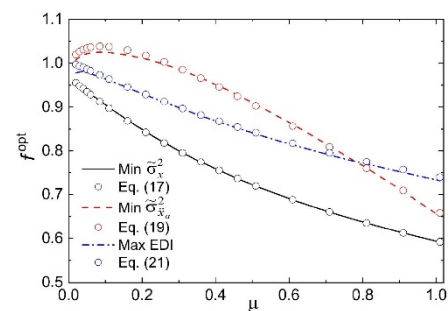


Fig. 3 Comparison of the optimum tuning frequency ratio of TMDI of base-isolated structure with proposed empirical equations

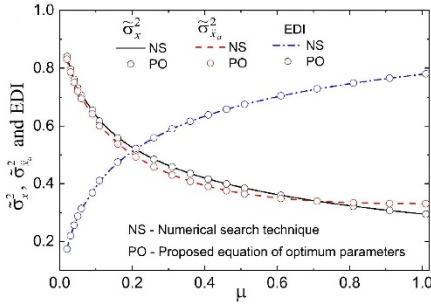


Fig. 4 Comparison of the optimum response of the base-isolated structure with TMDI using numerical search technique and with proposed empirical equations of optimum parameters

parameters using the proposed empirical equations.

The explicit mathematical equations obtained in the present study assume that the inertance mass ratio of the TMDI is less than unity and the damping ratio of the isolation system as 0.1. In addition, the μ_t is also kept as constant and equal to 0.01. The values of TMD mass ratio, inertance mass ratio, and damping considered in the isolated system cover parameter range encountered in the practical design of the TMDI system for damped base-isolated structure. The use of proposed equations beyond the above range may be susceptible to relative error. However, the same developed technique for the optimum TMDI parameters and explicit expressions can also be extended to different values of μ_t , various isolator damping, and different types of earthquake excitation.

4. Optimum TMDI under filtered white-noise excitation

Ground motions in earthquakes are inherently random and multi-dimensional. The ground motion can be described by a PSDF matrix and an intensity envelope function if the evolution of the frequency content with time is ignored. Clough and Penzien (2003) suggested that the PSDF of the earthquake excitation be as follows

$$S_{\ddot{x}_g}(\omega) = S_0 \left(\frac{1 + 4\xi_g^2(\omega/\omega_g)^2}{[1 - (\omega/\omega_g)^2]^2 + 4\xi_g^2(\omega/\omega_g)^2} \right) \times \left(\frac{(\omega/\omega_f)^4}{[1 - (\omega/\omega_f)^2]^2 + 4\xi_f^2(\omega/\omega_f)^2} \right) \quad (22)$$

where S_0 represents the constant PSDF of input white-noise random process; and ω_g and ξ_g denote the predominant frequency and damping ratio of the primary (soil media) filter; ω_f and ξ_f denote the secondary filter parameters. For the present study, three soil conditions are considered and Table 2 shows the relevant parameters from Kiureghian and Neuenhofer (1992).

The excitation has to be either white-noise or shot-noise for the stochastic response of any system using the state variable method described in Section 2.1, whereas the PSDF expressed by Eq. (22) is a non-white random process. This problem can be overcome by introducing shaping

Table 2 Filter parameters for different types of soil profiles

Site type	ω_g (rad/sec)	ω_f (rad/sec)	ξ_g	ξ_f
Firm soil	15	1.5	0.6	0.6
Medium soil	10	1.0	0.4	0.6
Soft soil	5	0.5	0.2	0.6

filters, which transform the random process \ddot{x}_g into the response of linear filters subjected to white-noise excitation as

$$\ddot{x}_g = \begin{Bmatrix} -\omega_f^2 & -2\xi_f\omega_f & \omega_g^2 & 2\xi_g\omega_g \end{Bmatrix} \begin{Bmatrix} u_f \\ \dot{u}_f \\ u_g \\ \dot{u}_g \end{Bmatrix} \quad (23)$$

$$\begin{Bmatrix} \dot{u}_f \\ \ddot{u}_f \\ \dot{u}_g \\ \ddot{u}_g \end{Bmatrix} = \begin{bmatrix} 0 & 1 & 0 & 0 \\ -\omega_f^2 & -2\xi_f\omega_f & \omega_g^2 & 2\xi_g\omega_g \\ 0 & 0 & 0 & 1 \\ 0 & 0 & -\omega_g^2 & -2\xi_g\omega_g \end{bmatrix} \begin{Bmatrix} u_f \\ \dot{u}_f \\ u_g \\ \dot{u}_g \end{Bmatrix} + \begin{Bmatrix} 0 \\ 0 \\ 0 \\ -\ddot{u}_0(t) \end{Bmatrix} \quad (24)$$

where u_g and u_f represent the displacement of primary and secondary filters, respectively; and $\ddot{u}_0(t)$ denotes the input white-noise random process with an intensity of the PSDF as S_0 . One should note that the Eqs. (23) and (24) provide the stationary PSDF of the \ddot{x}_g as that expressed by the Eq. (22).

Using the Eqs. (4), (23), and (24), new state-space first-order differential equations are written and the stochastic response of the base-isolated structure with TMDI for different soil profiles is obtained by using the method described in Section 2.1. The optimum parameters of the TMDI are obtained using the numerical search technique considering the isolation period $T_b = 2$ and 3 sec and $\xi_b = 0.1$.

A comparison of the optimum parameters of the TMDI system and the corresponding response of the base-isolated structure under the white-noise and filtered white-noise (i.e., firm, medium, and soft soils) models of earthquake excitation is shown in Fig. 5. The results are plotted for $T_b = 2$ sec and considering the optimality criterion as the minimization of the σ_x^2 and $\sigma_{\ddot{x}_a}^2$, and maximization of the *EDI*. It is seen from the figure that the optimized parameters are not much changing for the lower values of inertance-mass ratio (i.e., $\mu < 0.4$) subjected to the filtered white-noise model for the firm and medium soil conditions as compared with the corresponding white-noise excitation. However, as μ increases, the difference in optimum parameters grows, and it is more pronounced for the parameters of minimization of acceleration compared to the corresponding minimization of displacement and maximization of the *EDI*. Furthermore, when compared to the corresponding white-noise model, the TMDI's optimum parameters for the soft soil profile condition differ significantly. The corresponding optimum parameters and

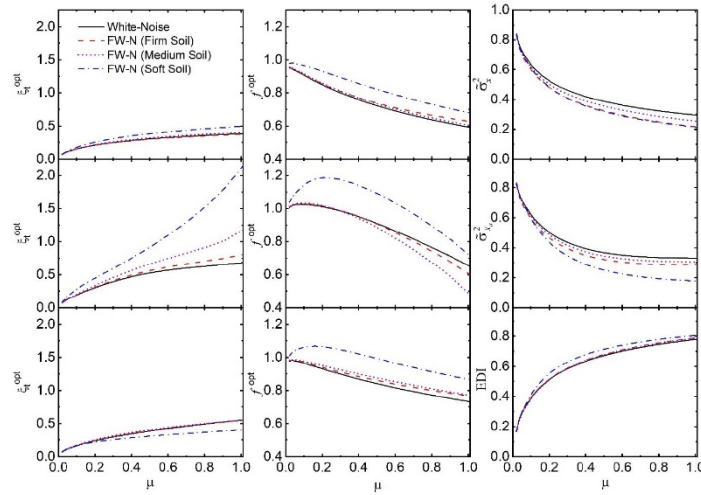


Fig. 5 Comparison of the optimum TMDI parameters and response of the base-isolated structure under white-noise and filtered white-noise excitations ($T_b = 2$ sec and $\xi_b = 0.1$)

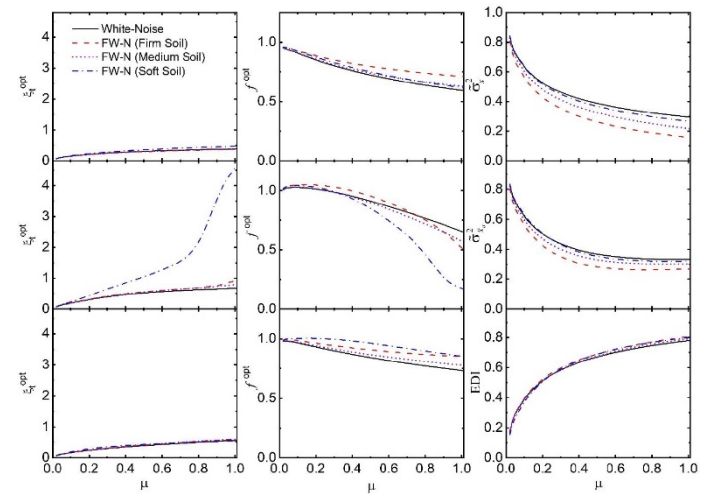


Fig. 6 Comparison of the optimum TMDI parameters and response of the base-isolated structure under white-noise and filtered white-noise excitations ($T_b = 3$ sec and $\xi_b = 0.1$)

optimized response for the $T_b = 3$ sec is shown in Fig. 6. The trend of variation of the optimum parameters and response in this figure remains the same as that observed in Fig. 5. The noticeable difference in the optimum parameters and optimized response for the isolation periods 2 and 3 sec is primarily observed for the soft soil conditions. With the increase of isolation period, there was less reduction in the displacement response and the corresponding damping ratio and tuning frequency were decreased. Also, there is a decrease in the reduction of the structural acceleration with the increase of isolation period and the corresponding damping ratio is increased and tuning frequency is decreased especially for higher inertia mass ratio. Thus, the optimized parameters of TMDI and corresponding response are influenced by the soil condition and the isolation frequency.

Figs. 5 and 6 indicated a specific trend for the minimization of the $\tilde{\sigma}_{\ddot{x}_a}^2$ under soft soil conditions. At a higher inertia ratio, the optimum TMDI damping is observed to be very high and the tuning frequency as low.

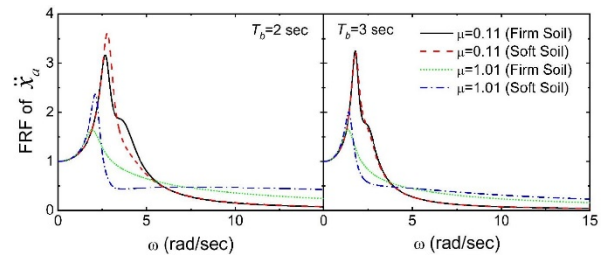


Fig. 7 Comparison of the FRF of \ddot{x}_a for different inertia ratios and soil profiles ($\xi_b = 0.1$)

Such behavior can be indicative of the optimized TMDI system as overdamped. To verify it, the frequency response function (FRF) of \ddot{x}_a for soft soil with $\mu = 1.01$ is plotted in Fig. 7 and compared with the corresponding firm soil and $\mu = 0.11$. The figure is revealing that the FRF of \ddot{x}_a for soft soil and $\mu = 1.01$ has a pre-dominant peak in the vicinity 1st natural frequency and after that, it remains

constant. This behavior indicating that the system is not overdamped and in fact, it is underdamped in the 1st mode and approaches the critical damping in the 2nd mode of vibration. This was further verified through the analysis of the complex modes and the same phenomenon was confirmed.

5. Response to real earthquake and cycloidal pulse excitation

TMDI was found to be very good in controlling the rigid base-isolated structure’s response under stationary white-noise and filtered white-noise excitation. However, it will be interesting to investigate its effectiveness under real earthquake and cycloidal pulse excitation and by considering base-isolated structure as flexible which will provide insight into the frequency contents of the superstructure acceleration and the tuning behavior of the TMDI. Fig. 8 shows a model of a flexible base-isolated building installed with the TMDI. For this building with TMDI, the governing equations of motion are

$$\mathbf{M}\ddot{\mathbf{x}}(t) + \mathbf{C}\dot{\mathbf{x}}(t) + \mathbf{K}\mathbf{x}(t) + \mathbf{D}\mathbf{F}_s(t) = -\mathbf{E}\ddot{x}_g(t) \quad (25)$$

where **M**, **C**, and **K** are the mass, damping, and stiffness matrices of the base-isolated building, respectively; **x**(*t*) represents the lateral displacements (relative to the ground) vector at time *t*; **D** is the location matrix for the vector of control forces **F**_{*s*}(*t*) produced by the inertial devices; **E** is the vector containing the vibrating masses; and $\ddot{x}_g(t)$ is the earthquake acceleration. The seismic response of the isolated building with TMDI is evaluated by numerically integrating the above equations of motion.

A five-story building with base isolation is selected for the present study and its parameters are taken from Kelly (1997). The parameters are: $m_1 = m_2 = m_3 = m_4 = m_5 = m_b$ (i.e., same mass at all floors and base raft locations). The inter-story stiffness of the floors is assumed as: $k_1 = 15k$, $k_2 = 14k$, $k_3 = 12k$, $k_4 = 9k$ and $k_5 = 5k$. The stiffness parameter *k* is chosen to give a fundamental period of the fixed base-superstructure of 0.4 seconds. The five natural frequencies

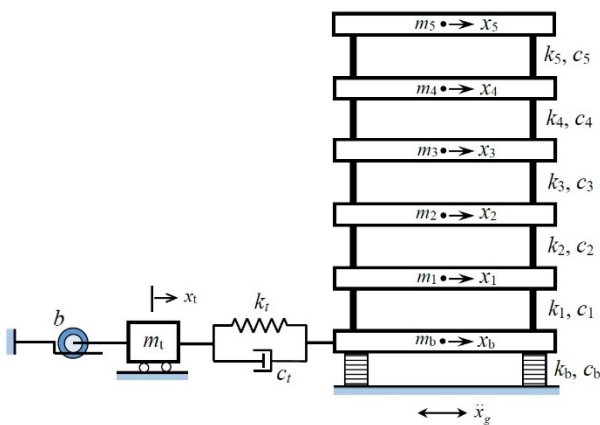


Fig. 8 Structural model of the flexible base-isolated building supplemented with TMDI

of the building with a fixed base measured in rad/sec are 15.71, 38.48, 60.84, 83.12, and 105.37. The superstructure’s damping matrix is built by assuming a modal damping ratio of 0.02 in all modes of vibration. The isolation damping ratio is selected as 10 percent. The selected response quantities are: the top floor absolute acceleration (\ddot{x}_5^a), relative base displacement (x_b), the relative displacement of the TMDI (x_i), and the base shear force of TMDI (F_{in} normalized with the total weight *W* of the isolated building).

5.1 Response under real earthquakes

Three recorded earthquake motions namely the north-south component of El-Centro, 1940 earthquake, N00E component of the 1989 Loma Prieta earthquake (recorded at Los Gatos Presentation Centre), and N90E component of 1994 Northridge earthquake (recorded at Sylmar Station) with 30 sec duration are selected. The peak ground acceleration of El-Centro, Loma Prieta, and Northridge earthquake motions are 0.34 *g*, 0.57 *g*, and 0.6 *g*, respectively (*g* denotes the acceleration due to gravity).

For the first example problem, a five-story building with an isolation system designed with an isolation period of 2 sec and supplemented with TMDI to control the top floor absolute acceleration is considered. The values of corresponding auxiliary mass, damping, and stiffness for TMDI and are taken from Table 1 for minimization of $\ddot{\sigma}_{x_a}^2$. The time variation of the top floor absolute acceleration, relative base displacement, the relative displacement of TMDI, and the base shear force of TMDI are shown in Fig. 9. The response is shown for the El-Centro, 1940 earthquake, and compared with the corresponding response without TMDI (referred to as BIS). The figure indicates that the peak top floor acceleration decreases for TMDI as compared to the corresponding BIS. The decrease in the peak acceleration is of the order of 12.5 percent. This figure is also revealing that the high-frequency components are present in the absolute acceleration of base-isolated structure with TMDI and may have some detrimental effects on high-frequency sensitive types of equipment. Further, the TMDI is also effective in reducing the base displacement and it is observed to be decreased by 20 percent. The maximum relative displacement in the TMDI is of the order of 0.15 m and the base shear force of TMDI is 6 percent of the total weight of the isolated structure.

The effects of the μ on the peak top floor acceleration, bearing displacement, the relative displacement of TMDI, and the base shear force of TMDI of the base-isolated building for different earthquakes are shown in Fig. 10. The figure shows that as the μ increases, the peak top floor acceleration, bearing displacement, and displacement in the TMDI decrease. On the other hand, as the μ increases, so does the peak TMDI force. The trend of results confirms that the TMDI is effective in controlling the structure’s response under real earthquake excitations when compared to the BIS (i.e., $\mu = 0$). These trends of the results are similar to those observed for the response under stationary earthquake excitation (refer to Figs. 4 to 6). Thus, the influence of μ on the response of base-isolated buildings with TMDI under deterministic time history analysis and the results obtained using a statistical approach under

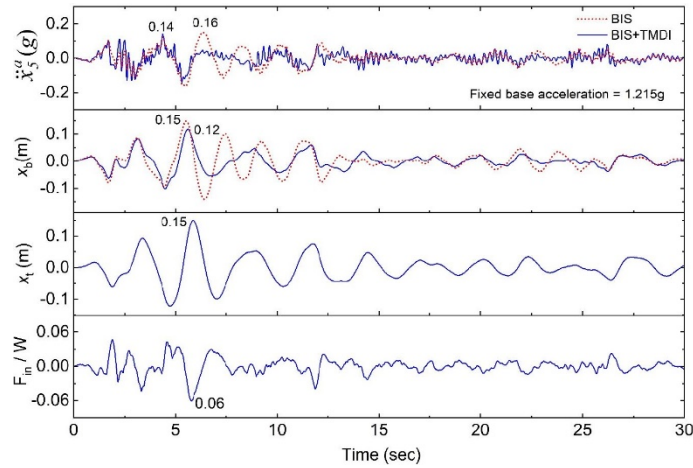


Fig. 9 Time variation of top floor absolute acceleration, relative base displacement, relative displacement of TMDI, and base shear force in the TMDI of five-story base-isolated structure under El-Centro, 1940 earthquake ($T_b = 2$ sec and $\mu = 0.41$)

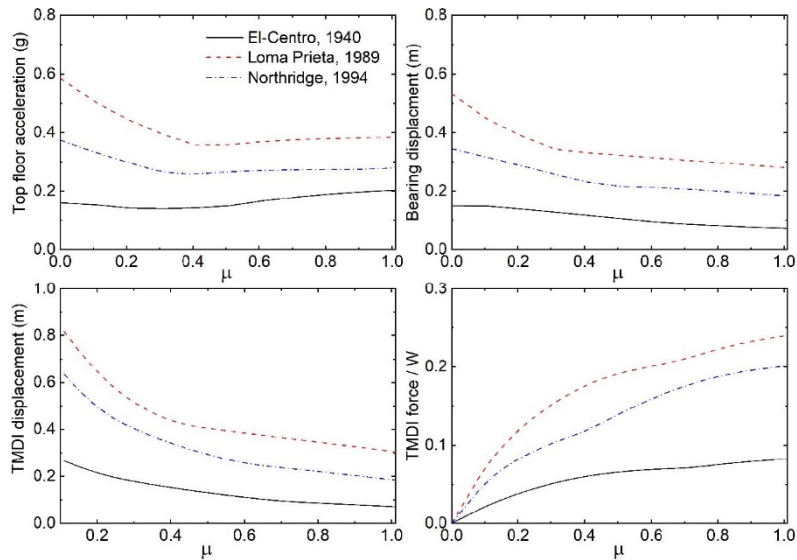


Fig. 10 Influence of the inertance of TMDI on the peak top floor absolute acceleration, relative base displacement, relative displacement of TMDI, and base shear force in the TMDI of five-story base-isolated structure ($T_b = 2$ sec)

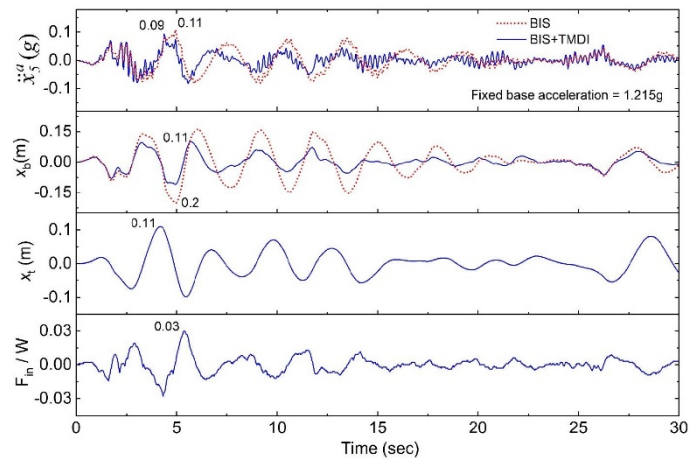


Fig. 11 Time variation of top floor absolute acceleration, relative base displacement, relative displacement of TMDI, and base shear force in the TMDI of five-story base-isolated structure under El-Centro, 1940 earthquake ($T_b = 3$ sec and $\mu = 0.41$)

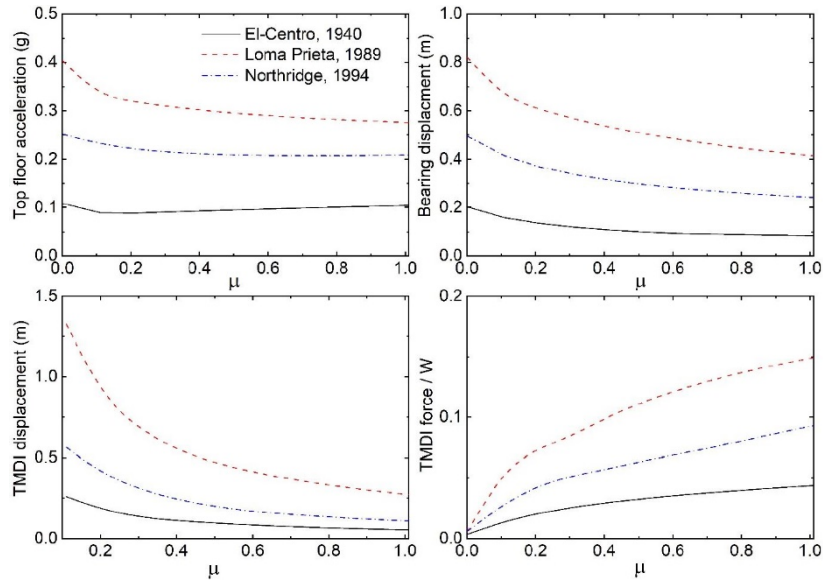


Fig. 12 Influence of the inertance of TMDI on the peak top floor absolute acceleration, relative base displacement, relative displacement of TMDI, and base shear force in the TMDI of a five-story base-isolated structure ($T_b = 3$ sec)

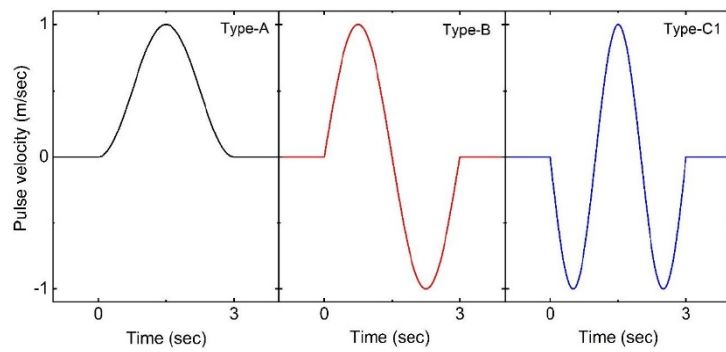


Fig. 13 Velocity variation of three distinct types of cycloidal pulses

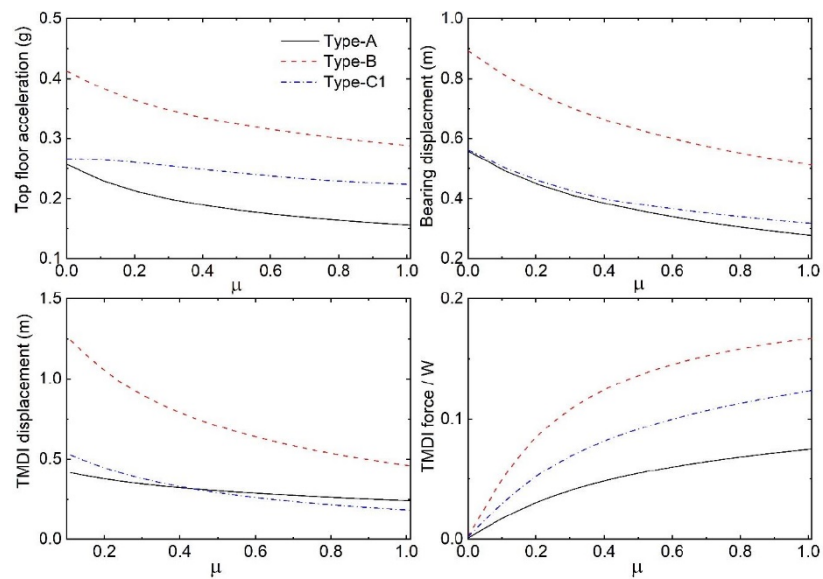


Fig. 14 Influence of the inertance of TMDI on the peak top floor absolute acceleration, relative base displacement, relative displacement of TMDI, and base shear force in the TMDI of a five-story base-isolated structure subjected to cycloidal pulses ($T_b = 3$ sec)

stochastic excitation are highly correlated.

For the second example problem, the five-story building with an isolation system designed with an isolation period of 3 sec and supplemented with TMDI to control the bearing displacement is considered. The values of corresponding auxiliary mass, damping, and stiffness for TMDI are taken from Table 1 for minimization of $\tilde{\sigma}_x^2$. Fig. 11 depicts the time variation of the top floor absolute acceleration, relative base displacement, relative displacement in the TMDI, and TMDI base shear force. Fig. 12 shows the effects of μ for different earthquakes on peak top floor acceleration and bearing displacement, displacement in the TMDI, and base shear force of TMDI of the base-isolated building. The trends in Figs. 11 and 12 are similar to those in Figs. 9 and 10, implying that a well-designed TMDI is effective in controlling the response of base-isolated structures.

5.2 Response under cycloidal pulses

Long-period pulses with high peak ground velocities characterize earthquake ground motions measured in the vicinity of an earthquake fault. Three distinct types of pulses namely Type-A, B, and C1 were found in the recorded ground motions (Makris and Chang 2000b). A half-cycle forward ground motion pulse is Type-A; a full-cycle forward-and-backward motion is Type-B; and a ground motion pulse with one main pulse in its displacement time history is Type-C1. The response of the base-isolated structure is significantly influenced if the pulse duration is close to the isolation period (Jangid and Kelly 2001, Rao and Jangid 2001, Jadhav and Jangid 2006, Mazza 2018). Fig. 13 shows the variation in the velocity of the three types of pulses having duration and amplitude as 3 sec and 1 m/sec, respectively. The response of a five-story isolated building with TMDI having an isolation period of 3 sec and subjected to the above pulses is shown in Fig. 14. The TMDI parameters are selected for the minimization of displacement to control the bearing displacements. It is observed that the TMDI reduces the bearing displacement and structural acceleration of the isolated structure under cycloidal pulses and performance is improved for higher inertance ratios. Thus, an optimally designed TMDI is effective in controlling the response of a base-isolated structure subjected to pulses of the same duration as the isolation period.

6. Conclusions

The seismic response of a base-isolated structure with TMDI is investigated when it is subjected to stationary random, real earthquake, and cycloidal pulses. A numerical searching technique is used to find the TMDI's optimum damping and tuning frequency ratio under stationary white-noise and filtered-white-noise excitation. Using a curve-fitting technique, explicit formulae for TMDI damping and tuning frequency are then derived, which can be used in practical applications. The following conclusions can be drawn from the trends of the current study's findings:

- (1) The effectiveness of an optimally designed TMDI in controlling the displacement and acceleration

response of the base-isolated structure is observed to increase with higher inertance-mass ratio. However, for inertance-mass ratios greater than 0.4, the reduction in isolated structure response was only marginal.

- (2) For a base-isolated structure, the optimal TMDI parameters obtained by minimizing the acceleration are generally higher than those obtained by minimizing the displacement. The optimum parameters for maximization of the EDI are observed to be bounded between the optimum parameters for minimization of the isolated structure's displacement and acceleration response for the practical range of the inertance-mass ratio.
- (3) The curve-fitting scheme with minimum mean square error used to derive explicit expressions for optimum TMDI parameters fit well with the values obtained from the numerical searching technique.
- (4) The optimized TMDI parameters are not much altered for lower values of inertance-mass ratio (i.e., $\mu < 0.4$) under the filtered white-noise model for the firm and medium soil condition as compared with the white-noise excitation. However, for a higher inertance ratio, the optimized parameters and response are influenced by the soil condition and the isolation frequency.
- (5) An optimally designed TMDI is found to be effective in controlling the response of the multi-story base-isolated buildings under real earthquake excitation.
- (6) The optimal TMDI is also effective in controlling the response of a base-isolated structure to cycloidal pulses with a duration close to the isolation period.

References

- Bakre, S.V. and Jangid, R.S. (2007), "Optimum parameters of tuned mass damper for damped main system", *Struct. Control Health Monitor.*, **14**, 448-470. <https://doi.org/10.1002/stc.166>
- Bandivadekar, T.P. and Jangid, R.S. (2013), "Optimization of multiple tuned mass dampers for vibration control of system under external excitation", *J. Vib. Control*, **19**, 1854-1871. <https://doi.org/10.1177/1077546312449849>
- Barredo, E., Mendoza Larios J.G., Mayén, J., Flores-Hernández, A.A., Colín, J. and Arias Montiel, M. (2019), "Optimal design for high-performance passive dynamic vibration absorbers under random vibration", *Eng. Struct.*, **195**, 469-489. <https://doi.org/10.1016/j.engstruct.2019.05.105>
- Cao, L. and Li, C. (2019), "Tuned tandem mass dampers-inerters with broadband high effectiveness for structures under white noise base excitations", *Struct. Control Health Monitor.*, **26**(4), e2319. <https://doi.org/10.1002/stc.2319>
- Cao, L., Li, C. and Chen, X. (2020), "Performance of multiple tuned mass dampers-inerters for structures under harmonic ground acceleration", *Smart Struct. Syst., Int. J.*, **26**(1), 49-61. <https://doi.org/10.12989/sss.2020.26.1.049>
- Clough, R.W. and Penzien, J. (2003), *Dynamics of Structures*, (3rd Edition), Berkeley, CA, USA, Computers and Structures.
- De Angelis, M., Giaralis, A., Petrini, F. and Pietrosanti, D. (2019), "Optimal tuning and assessment of inertial dampers with grounded inerter for vibration control of seismically excited base-isolated systems", *Eng. Struct.*, **196**, 109250.

- <https://doi.org/10.1016/j.engstruct.2019.05.091>
- De Domenico, D. and Ricciardi, G. (2018a), "An enhanced base isolation system equipped with optimal tuned mass damper inerter (TMDI)", *Earthq. Eng. Struct. Dyn.*, **47**(5), 1169-1192. <https://doi.org/10.1002/eqe.3011>
- De Domenico, D. and Ricciardi, G. (2018b), "Improving the dynamic performance of base-isolated structures via tuned mass damper and inerter devices: A comparative study", *Struct. Control Health Monitor.*, **25**(10), e2234. <https://doi.org/10.1002/stc.2234>
- De Domenico, D., Ricciardi, G. and Zhang, R. (2020), "Optimal design and seismic performance of tuned fluid inerter applied to structures with friction pendulum isolators", *Soil Dyn. Earthq. Eng.*, **132**, 106099. <https://doi.org/10.1016/j.soildyn.2020.106099>
- Di Matteo, A., Masnata, C. and Pirrotta, A. (2019), "Simplified analytical solution for the optimal design of Tuned Mass Damper Inerter for base isolated structures", *Mech. Syst. Signal Process.*, **134**, 106337. <https://doi.org/10.1016/j.ymsp.2019.106337>
- Garrido, H., Curadelli, O. and Ambrosini, D. (2013), "Improvement of tuned mass damper by using rotational inertia through tuned viscous mass damper", *Eng. Struct.*, **56**, 2149-2153. <https://doi.org/10.1016/j.engstruct.2013.08.044>
- Hu, Y., Chen, M.Z., Shu, Z. and Huang, L. (2015), "Analysis and optimisation for inerter-based isolators via fixed-point theory and algebraic solution", *J. Sound Vib.*, **346**, 17-36. <https://doi.org/10.1016/j.jsv.2015.02.041>
- Hwang, J.-S., Kim, J. and Kim, Y.-M. (2007), "Rotational inertia dampers with toggle bracing for vibration control of a building structure", *Eng. Struct.*, **29**(6), 1201-1208. <https://doi.org/10.1016/j.engstruct.2006.08.005>
- Jadhav, M.B. and Jangid, R.S. (2006), "Response of base-isolated liquid storage tanks to near-fault motions", *Struct. Eng. Mech., Int. J.*, **23**(6), 615-634. <https://doi.org/10.12989/sem.2006.23.6.615>
- Jangid, R.S. and Kelly, J.M. (2001), "Base isolation for near-fault motions", *Earthq. Eng. Struct. Dyn.*, **30**(5), 691-707. <https://doi.org/10.1002/eqe.31>
- Kataria, N.P. and Jangid, R.S. (2016), "Seismic protection of the horizontally curved bridge with semi-active variable stiffness damper and isolation system", *Adv. Struct. Eng.*, **19**(7), 1103-1117. <https://doi.org/10.1177/1369433216634477>
- Kelly, J.M. (1997), *Earthquake-Resistant Design with Rubber*, (2nd Ed.), London, UK, Springer-Verlag.
- Kiureghian, A.D. and Neuenhofer, A. (1992), "Response spectrum method for multi-support seismic excitations", *Earthq. Eng. Struct. Dyn.*, **21**(8), 713-740. <https://doi.org/10.1002/eqe.4290210805>
- Lazar, I.F. (2014), "Using an inerter-based device for structural vibration suppression", *Earthq. Eng. Struct. Dyn.*, **43**(8), 1129-1147. <https://doi.org/10.1002/eqe.2390>
- Li, Y. and Li, J. (2019), "Overview of the development of smart base isolation system featuring magnetorheological elastomer", *Smart Struct. Syst., Int. J.*, **24**(1), 37-52. <https://doi.org/10.12989/sss.2019.24.1.037>
- Li, C., Chang, K., Cao, L. and Huang, Y. (2021), "Performance of a nonlinear hybrid base isolation system under the ground motions", *Soil Dyn. Earthq. Eng.*, **143**, 106589. <https://doi.org/10.1016/j.soildyn.2021.106589>
- Lin, P.Y., Roschke, P.N. and Loh, C.H. (2006), "Hybrid base-isolation with magnetorheological damper and fuzzy control", *Struct. Control Health Monitor.*, **14**(3), 384-405. <https://doi.org/10.1002/stc.163>
- Madhekar, S.N. and Jangid, R.S. (2009), "Variable dampers for earthquake protection of benchmark highway bridges", *Smart Mater. Struct.*, **18**(11), 115011. <https://doi.org/10.1088/0964-1726/18/11/115011>
- Makris, N. and Chang, S.-P. (2000a), "Effect of viscous, viscoelastic and friction damping on the response of seismic isolated structures", *Earthq. Eng. Struct. Dyn.*, **29**(1), 85-107. [https://doi.org/10.1002/\(SICI\)1096-9845\(200001\)29:1%3C85::AID-EQE90%3E3.0.CO;2-N](https://doi.org/10.1002/(SICI)1096-9845(200001)29:1%3C85::AID-EQE90%3E3.0.CO;2-N)
- Makris, N. and Chang, S.-P. (2000b), "Response of damped oscillators to cycloidal pulses", *J. Eng. Mech.*, **126**(2), 123-131. [https://doi.org/10.1061/\(ASCE\)0733-9399\(2000\)126:2\(123\)](https://doi.org/10.1061/(ASCE)0733-9399(2000)126:2(123))
- Makris, N. and Moghimi, G. (2019), "Displacements and forces in structures with inerters when subjected to earthquakes", *J. Struct. Eng.*, **145**(2), 04018260. [https://doi.org/10.1061/\(ASCE\)ST.1943-541X.0002267](https://doi.org/10.1061/(ASCE)ST.1943-541X.0002267)
- Marian, L. and Giaralis, A. (2014), "Optimal design of a novel tuned mass damper-inerter (TMDI) passive vibration control configuration for stochastically support-excited structural systems", *Probabil. Eng. Mech.*, **38**, 156-164. <https://doi.org/10.1016/j.probengmech.2014.03.007>
- Masri, S.F. and Caffrey, J.P. (2017), "Transient response of a SDOF system with an inerter to nonstationary stochastic excitation", *J. Appl. Mech.*, **84**(4), 041005. <https://doi.org/10.1115/1.4035930>
- Matsagar, V.A. and Jangid, R.S. (2008), "Base isolation for seismic retrofitting of structures", *Pract. Period. Struct. Des. Constr.*, **13**(4), 175-185. [https://doi.org/10.1061/\(ASCE\)1084-0680\(2008\)13:4\(175\)](https://doi.org/10.1061/(ASCE)1084-0680(2008)13:4(175))
- Mazza, F. (2018), "Seismic demand of base-isolated irregular structures subjected to pulse-type earthquakes", *Soil Dyn. Earthq. Eng.*, **108**, 111-129. <https://doi.org/10.1016/j.soildyn.2017.11.030>
- Mazza, F. (2019), "Effects of the long-term behaviour of isolation devices on the seismic response of base-isolated buildings", *Struct. Control Health Monitor.*, **26**(4), e2331. <https://doi.org/10.1002/stc.2331>
- Mazza, F. (2021), "Base-isolation of a hospital pavilion against in-plane-out-of-plane seismic collapse of masonry infills", *Eng. Struct.*, **228**, 111504. <https://doi.org/10.1016/j.engstruct.2020.111504>
- Nagarajaiah, S. and Sen, D. (2020), "Apparent-weakening by adaptive passive stiffness shaping along the height of multistory building using negative stiffness devices and dampers for seismic protection", *Eng. Struct.*, **220**, 110754. <https://doi.org/10.1016/j.engstruct.2020.110754>
- Patil, V.B. and Jangid, R.S. (2011), "Optimum multiple tuned mass dampers for the wind excited benchmark building", *J. Civil Eng. Manag.*, **17**(4), 540-557. <https://doi.org/10.3846/13923730.2011.619325>
- Pietrosanti, D., De Angelis, M. and Basili, M. (2017), "Optimal design and performance evaluation of systems with Tuned Mass Damper Inerter (TMDI)", *Earthq. Eng. Struct. Dyn.*, **46**(8), 1367-1388. <https://doi.org/10.1002/eqe.2861>
- Rao, P.B. and Jangid, R.S. (2001), "Performance of sliding systems under near-fault motions", *Nuclear Eng. Des.*, **203**, 259-272. [https://doi.org/10.1016/S0029-5493\(00\)00344-7](https://doi.org/10.1016/S0029-5493(00)00344-7)
- Reigles, D.G. and Symans, M.D. (2006), "Supervisory fuzzy control of a base-isolated benchmark building utilizing a neuro-fuzzy model of controllable fluid viscous dampers", *Struct. Control Health Monitor.*, **13**, 724-747. <https://doi.org/10.1002/stc.108>
- Roberts, J.B. and Spanos, P.D. (1990), *Random Vibration and Statistical Linearization*, Chichester, UK, Wiley.
- Salvi, J. and Rizzi, E. (2016), "Closed-form optimum tuning formulas for passive tuned mass dampers under benchmark excitations", *Smart Struct. Syst., Int. J.*, **17**(2), 231-256. <https://doi.org/10.12989/sss.2016.17.2.231>
- Spencer Jr, B.F. and Nagarajaiah, S. (2003), "State of the art of structural control", *J. Struct. Eng.*, **129**(7), 845-856. [https://doi.org/10.1061/\(ASCE\)0733-9445\(2003\)129:7\(845\)](https://doi.org/10.1061/(ASCE)0733-9445(2003)129:7(845))

- Tigli, O.F. (2012), "Optimum vibration absorber (tuned mass damper) design for linear damped systems subjected to random loads", *J. Sound Vib.*, **331**(13), 3035-3049.
<https://doi.org/10.1016/j.jsv.2012.02.017>
- Tiong, P.L.Y., Kelly, J.M. and Or, T.T. (2017), "Design approach of high damping rubber bearing for seismic isolation", *Smart Struct. Syst., Int. J.*, **20**(3), 303-309.
<https://doi.org/10.12989/sss.2017.20.3.303>
- Wang, B., Zhu, S. and Casciati, F. (2020), "Experimental study of novel self-centering seismic base isolators incorporating superelastic shape memory alloys", *J. Struct. Eng.*, **146**(7), 04020129.
[https://doi.org/10.1061/\(ASCE\)ST.1943-541X.0002679](https://doi.org/10.1061/(ASCE)ST.1943-541X.0002679)
- Wen, Y., Chen, Z. and Hua, X. (2017), "Design and evaluation of tuned inerter-based dampers for the seismic control of MDOF structures", *J. Struct. Eng.*, **143**(4), 04016207.
[https://doi.org/10.1061/\(ASCE\)ST.1943-541X.0001680](https://doi.org/10.1061/(ASCE)ST.1943-541X.0001680)